# Supplemental material

Gómez-Sánchez et al., https://doi.org/10.1083/jcb.201710116

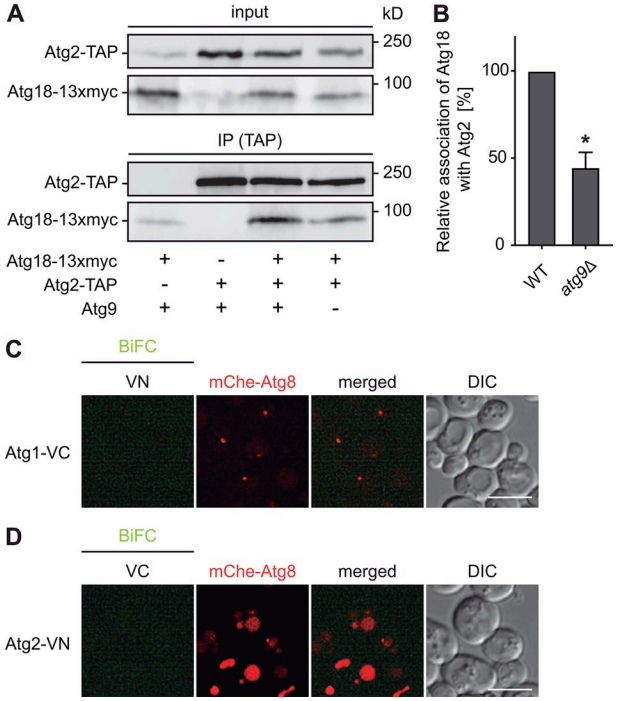


Figure S1. **Atg2–Atg18 complex stability is compromised in *atg9Δ* cells. (A)** Cell extracts from strains expressing either Atg18-13×myc (RSGY015) or Atg2-TAP (RSGY016) or cells carrying both fusion proteins but with (WT; RSGY012) or without *ATG9* (*atg9Δ*; RGY562) were subjected to coimmunoprecipitation experiments as performed in Fig. 2 E but using a lysis buffer without $MgCl_2$. **(B)** Quantification of the experiment shown in A. The ratio between Atg18–13×myc/Atg2-TAP was determined by quantifying the intensity of the corresponding bands and subsequently expressing it relative to the cells carrying Atg9. Error bars correspond with the SD of two independent experiments. The asterisk highlights significant differences with the cells expressing Atg9. **(C and D)** The Atg1-VC and Atg2-VN fusions did not interact with cytoplasmic VN and VC fragments, respectively. **(C)** A strain (RHY040) expressing endogenous Atg1–VC and *ATG2* promoter-driven VN and carrying the mCherryV5-Atg8 construct was grown to an early log phase before being nitrogen starved for 3 h in SD-N and imaged. **(D)** Cells (RHY038) expressing endogenous Atg2–VN and *ATG1* promoter-driven VN and carrying the mCherryV5-Atg8 construct were processed in the same way. DIC, differential interference contrast. Bars, 5 µm.

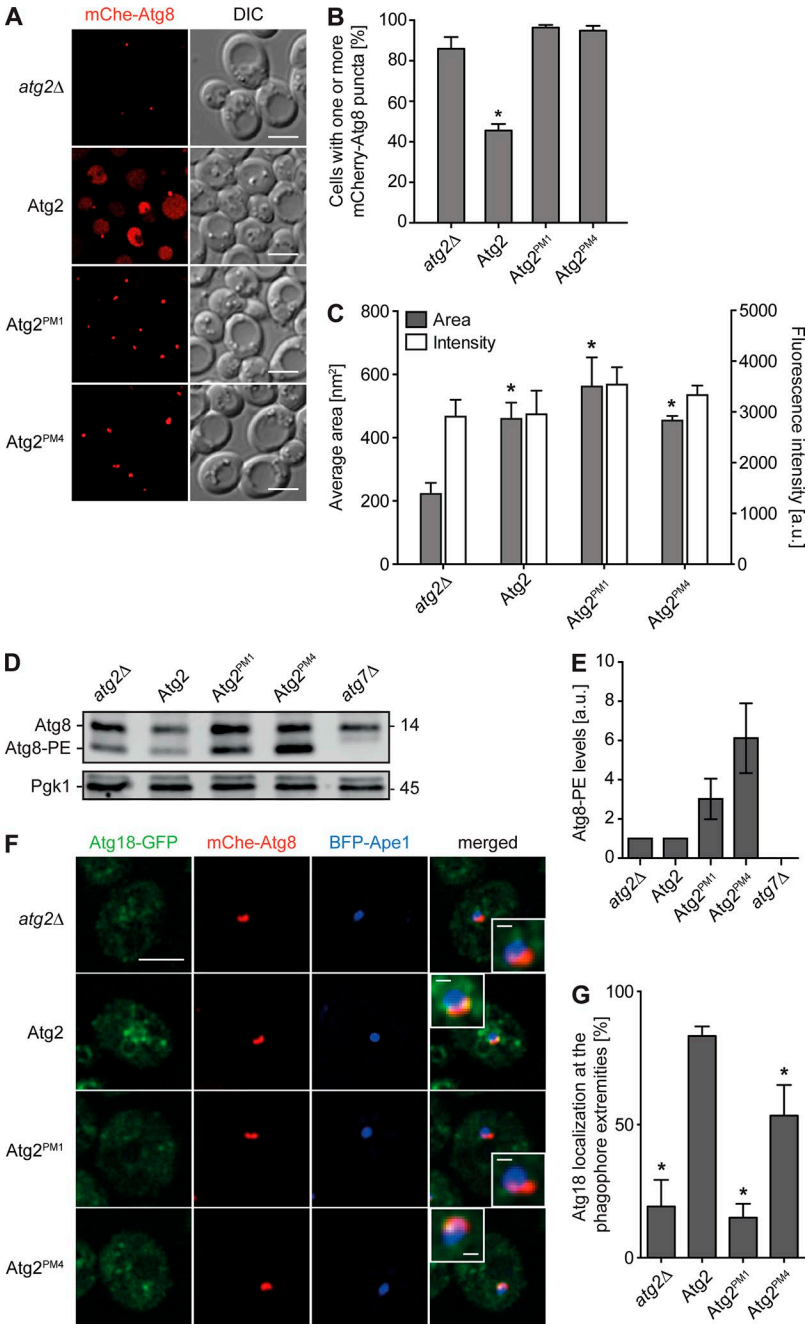


Figure S2. **Atg2$^{PM1}$ and Atg2$^{PM4}$ mutants block phagophore expansion. (A)** The *atg2Δ* knockout in the W303 background expressing mCherryV5-Atg8 (RSGY040) was transformed with integrative plasmids expressing TAP-tagged versions of Atg2 (pATG2-TAP(405); RSGY041), Atg2$^{PM1}$ (pATG2$^{PM1}$-TAP(405); RSGY042), or Atg2$^{PM4}$ (pATG2$^{PM4}$-TAP(405); RSGY043). Strains were grown in YPD to an early log phase before being nitrogen starved in SD-N for 3 h and imaged by fluorescence microscopy. DIC, differential interference contrast. Bars, 5 µm. **(B)** Quantification of percentages of cells that presented at least one mCherryV5-Atg8 punctum in A. The asterisk indicates a significant difference with the *atg2Δ* knockout. **(C)** Quantification of the mean size in nm2 and intensity of the fluorescent signal in a.u. of mCherryV5-Atg8 puncta depicted in A. Data analysis was performed as described in Materials and methods. Asterisks indicate significant differences with *atg2Δ* cells. **(D)** The *atg2Δ* knockout in the W303 background (RSGY053) was transformed with integrative plasmids expressing TAP-tagged versions of Atg2 (pATG2-TAP(405); RSGY052), Atg2$^{PM1}$ (pATG2$^{PM1}$-TAP(405); RSGY054), or Atg2$^{PM4}$ (pATG2$^{PM4}$-TAP(405); RSGY055), and the resulting strains were grown to a log phase in YPD before being nitrogen starved in SD-N for 1 h. The *atg7Δ* knockout (VDY101) was used as a control for a mutant unable to generate Atg8-PE. Proteins were precipitated with TCA and analyzed by Western blotting using the anti-Atg8 antibody. Western blot staining with anti-Pgk1 antibodies was used as the loading control. Molecular weights are given in kilodaltons. **(E)** Quantification of the levels of Atg8-PE in a.u. in the experiment shown in C. **(F)** Examination of Atg18-GFP distribution on the phagophores adjacent to giant Ape1 by fluorescence microscopy. The *atg2Δ* strain expressing Atg18-GFP and mCherry-Atg8 carrying the empty plasmid pRS405 (*atg2Δ*; RGY528) or integrative plasmids expressing TAP-tagged versions of Atg2 (RGY529), Atg2$^{PM1}$ (RGY530), or Atg2$^{PM4}$ (RGY531) were transformed with the pDP245 plasmid and analyzed as described in Materials and methods. Bars: (main images) 2 µm; (insets) 300 nm. **(G)** Statistical evaluation of the phagophore displaying Atg18-GFP at their extremities. Asterisks indicates significant differences with the strain carrying WT Atg2. All graphs represent means of three experiments ± SD.

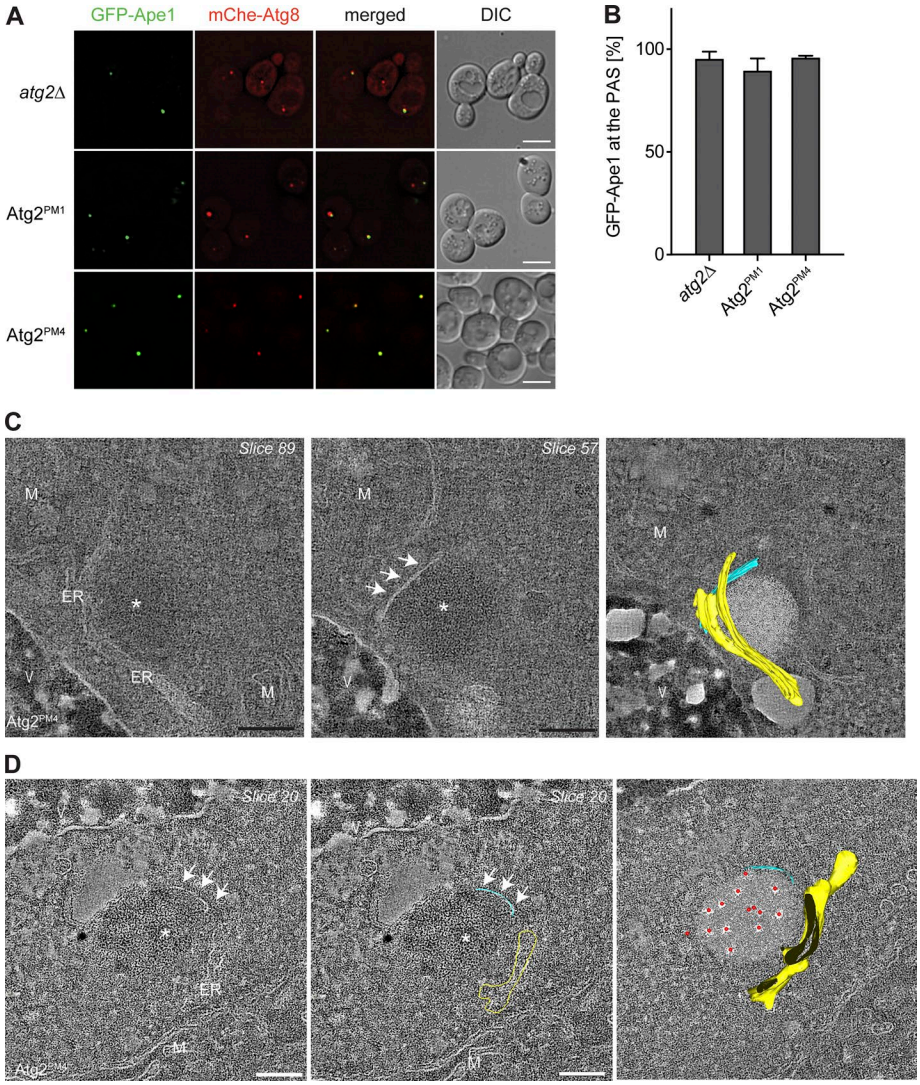


Figure S3. **The Ape1 oligomer localizes to the PAS in absence of Atg2 and in cells expressing Atg2$^{PM1}$ or Atg2$^{PM4}$. (A)** The *atg2Δ* strains expressing mCherryV5-Atg8 and carrying an integrative empty plasmid pRS405 (*atg2Δ*; RSGY024) or expressing Atg2$^{PM1}$ (RSGY025) or Atg2$^{PM4}$ (RSGY026) were transformed with a plasmid expressing GFP-Ape1 (pTS466) and grown in SMD at 30°C to a log phase before triggering autophagy by nitrogen starvation in SD-N for 1 h. Cells were imaged after autophagy induction. DIC, differential interference contrast. Bars, 5 µm. **(B)** Percentages of GFP-Ape1 colocalizing with the PAS marker protein mCherryV5-Atg8 in the experiment shown in A. The graph represents the mean of two experiments ± SD. **(C)** Single tomographic slices showing either the ER (z slice 89) or the phagophore (z slice 57, arrows) tethered to the Ape1 oligomer plus the model of the three structures through the tomogram. **(D)** Single tomographic slice (z slice 20, arrows) showing the ER and the phagophore (arrows) surrounding the prApe1 oligomer. The complete modeling is shown in the respective right panels. M, mitochondrion; V, vacuole. ER is in yellow; phagophore is in light blue; asterisks indicate Ape1 oligomers; red spheres indicate immunogold labeling. Black bars, 184 nm; white bars, 156 nm. The entire tomograms and models of the tomographic slices shown in A and B are presented in Videos 5 and 6, respectively.

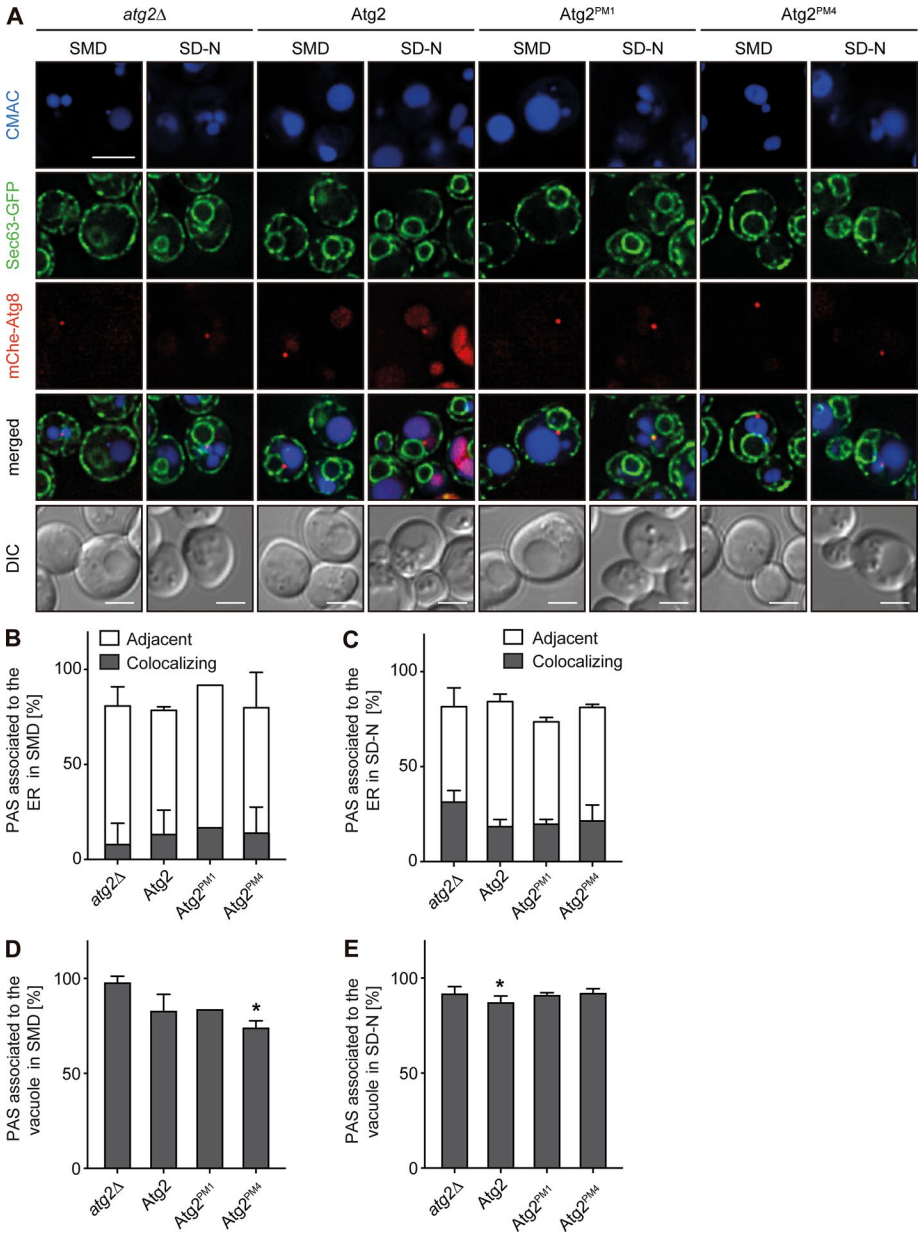


Figure S4. **The PAS is adjacent to the ER and vacuole in *atg2* mutants. (A)** The *atg2Δ* strain expressing Sec63-GFP and mCherry-Atg8 carrying the empty plasmid pRS414 (*atg2Δ*; RGY296) or a vector expressing Atg2 (RGY303), Atg2$^{PM1}$ (RGY304), or Atg2$^{PM4}$ (RGY305) were grown in YPD at 30°C to a log phase before stimulating autophagy by nitrogen starvation in SD-N for 3 h. Cells were imaged before and after autophagy induction. Cells were also incubated with CMAC dye for 10 min before being analyzed to label the vacuolar lumen. A single focal plane of a representative is shown. DIC, differential interference contrast. Bars, 5 µm. **(B and C)** Percentage of the PAS adjacent or colocalizing with the ER in growing (B) and autophagy-inducing (C) conditions in the experiment shown in A. **(D and E)** Percentage of PAS associated to the vacuole in growing (D) and autophagy-inducing (E) conditions in the experiment shown in A. Data represent the mean of two independent experiments ± SD. Asterisks highlight significant differences with the strain expressing *atg2Δ* cells.

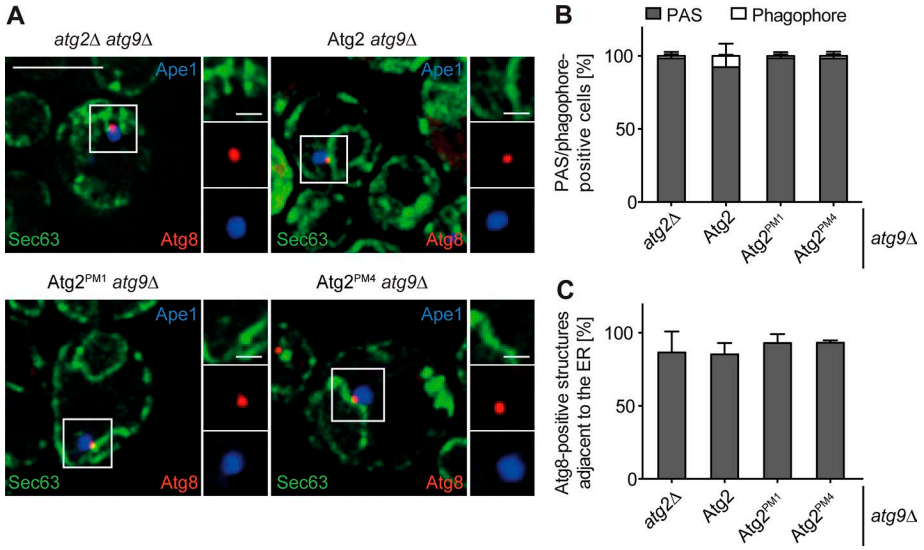


Figure S5. **Role of Atg9 in the phagophore formation. (A)** The *atg2Δ atg9Δ* mutant expressing Sec63-GFP and mCherry-Atg8 (RHY034) was transformed with both pDP245 and the pRS416 empty vector or a plasmid expressing Atg2 (pYCG_YNL242w), Atg2$^{PM1}$ (pYCG_YNL242w_PM1), or Atg2$^{PM4}$ (pY- CG_YNL242w_PM4). The resulting strains were grown in SMD to an early log phase before to induce the formation of giant Ape1 as described in Materials and methods and to image the cells. Bars: (main images) 5 µm; (insets) 1 µm. **(B)** Percentage of cells displaying a PAS or a phagophore in the experiment shown in A. **(C)** Percentage of Atg8-positive PAS/phagophore adjacent to the ER. Data represent the mean of three independent experiments ± SD.

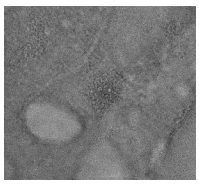

Video 1. **3D reconstruction with modeling of an Ape1 oligomer in the *atg2Δ* mutant, with adjacent ER.** Gray sphere, Ape1 ologomer; yellow, ER. Gold particles are indicated with red circles.

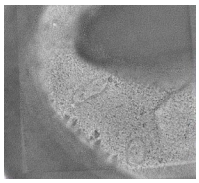

Video 2. **3D reconstruction with modeling of an Ape1 oligomer in the *atg2Δ* strain, with an ER tethered with a single *point of contact*.** Gray sphere, Ape1 oligomer; yellow, ER. Gold particles are indicated with red circles.

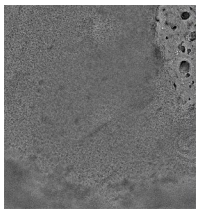

Video 3. **3D reconstruction with modeling of an Ape1 oligomer in Atg2$^{PM1}$-expressing cells, with an ER tethered with a *surface contact*.** Gray sphere, Ape1 oligomer; yellow, ER. Gold particles are indicated with red circles.

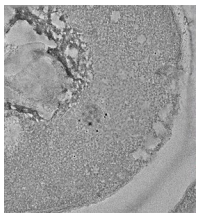

Video 4. **3D reconstruction with modeling of an Ape1 oligomer in Atg2$^{PM1}$-expressing cells, with an ER tethered with *enwrapping*.** Gray sphere, Ape1 oligomer; yellow, ER. Gold particles are indicated with red circles.

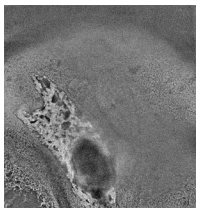

Video 5. **3D reconstruction with modeling of an Ape1 oligomer in Atg2$^{PM4}$-expressing cells, revealing the presence of a phagophore.** Gray sphere, Ape1 oligomer; yellow, ER; blue, phagophore. Gold particles are indicated with red circles.

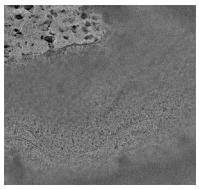

Video 6. **3D reconstruction with modeling of an Ape1 oligomer in Atg2$^{PM4}$-expressing cells, revealing the presence of a phagophore.** Gray sphere, Ape1 oligomer; yellow, ER; blue, phagophore. Gold particles are indicated with red circles.

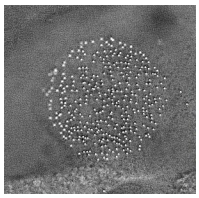

Video 7. **3D reconstruction of a giant Ape1 oligomer in Atg2$^{PM1}$-expressing cells, with ER in close association.** Gold particles are seen as small white spheres.

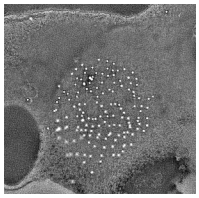

Video 8. **3D reconstruction of a giant Ape1 oligomer in Atg2$^{PM4}$-expressing cells, with ER in close association.** Gold particles are seen as small white spheres.

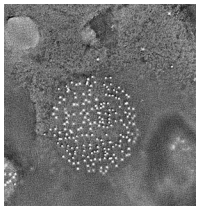

Video 9. **3D reconstruction of a giant Ape1 oligomer in the WT strain showing the ER having a *point contact*.** Gold particles are seen as small white spheres.